CHEMPLUSCHEM

DOI: 10.1002/cplu.201200070

Plasma Synthesis of Surface-Functionalized Graphene-Based Platinum Nanoparticles: Highly Active Electrocatalysts as Electrodes for Direct Methanol Fuel Cells

Qi Wang,[a] Mingming Song,[a] Changlun Chen,[a] Wenping Hu,[b] and Xiangke Wang*[a]

With their high energy-conversion efficiency, low emission, and high power density, direct methanol fuel cells (DMFC) have drawn tremendous attention in recent years. One of the key issues is to improve the oxygen reduction reaction (ORR) kinetics at the cathode.[1] Traditional Pt catalysts have already been applied and numerous substitutes have been developed to expand DMFC application such as nonprecious metal,[2] cytochrome c oxidase,[3] carbon-supported Pt–Au alloys,[4] nitrogen-doped carbon nanotubes,[5] and mesoporous graphitic arrays.[6]

Graphene, owing to its unique 2D structure, high surface area, and electrical conductivity has been used as the support to synthesize graphene-based precious metal nanoparticles (NPs) for application in DMFC. To date, graphene-based metal NPs have been mostly synthesized in solution or gas phase. Two strategies were mainly adopted: 1) to firstly synthesize a graphene-based metal salt , then the precious metals were deposited on graphene by metal salt reduction; or 2) precious metals were firstly deposited on graphene oxide (GO) followed by GO reduction to graphene.[7] The reduction usually needs chemical reducing reagents, such as methanol, ethanol, hydrazine hydrate, $NaBH_4$, trisodium citrate, or formaldehyde.[8] Sometimes, surfactants were used to control particle growth, but adversely affected its properties.[9] In the gas phase, metal NPs are produced by electric arc-discharge,[10] flame-spray pyrolysis,[11] pulsed laser,[12] or microwave plasma.[13] However, these techniques are energy consuming and complex, furthermore, the extreme conditions such as high temperature and expensive equipment limit their application on a large scale .[14] Recently, researchers have reported facile methods[15] to prepare metal NPs on graphene such as electrochemical reduction, ultrasonication, or microwave-assisted heating. In addition, some reports presented the preparation of graphene–Pt or functionalized graphene–Pt nanocomposites.[16] However, it still remains a great challenge to synthesize homogeneous grapheme-supported Pt NP nanocomposites with uniform size through simple, cost-effective, surfactant-free routes under mild conditions.

Herein, we presented a novel and facile mild plasma approach to synthesize Pt NPs on H-doped graphene (GH) and N-doped graphene (GHA) in the gas phase (Figure 1). The GH and GHA were prepared by reduction of GO in hydrogen and ammonia plasma, respectively. The GH-based Pt NPs (Pt/GH) and GHA-based Pt NPs (Pt/GHA) were prepared by simultaneous reduction of GH and H_2PtCl_6 or GHA and H_2PtCl_6 under hydrogen plasma, respectively. All the plasma was generated in a home-made system (see the Experimental Section for details). High-energy electrons in plasma created a large number of reactive and radical species as a result of decomposing source gases. All reactions such as doping, functionalization, and reduction were carried out under mild conditions (at ≈30 °C). The plasma technique is simple and environmental friendly, it avoids large amounts of chemicals in the doping and reduction processes. The electrocatalytic activities of the two plasma-treated catalysts were studied, and the Pt/GHA was applied as the cathode in DMFC—the performance of which was compared with the Pt/GH and other reported catalysts. To the best of our knowledge, this is the first time that graphene doping has combined the reduction of both graphene oxide and the metal precursor. This approach thus demonstrates that the mild plasma technique could be a facile strategy to support doping and functionalization as well as highly active metal NP growth on carbonaceous or other supports.

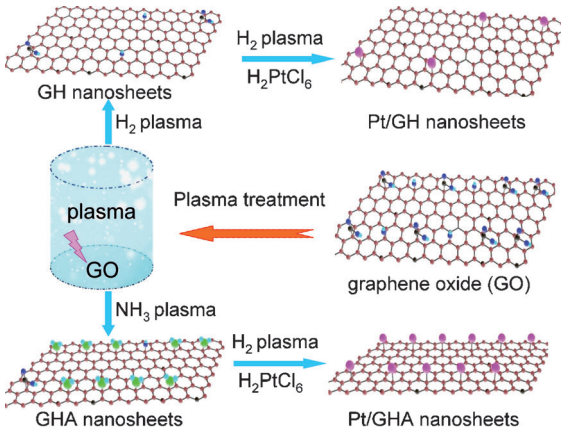

Figure 1. Synthesis of Pt/GH and Pt/GHA by the plasma approach.

Scanning electron microscopy (SEM) and transmission electron microscopy (TEM) images of the Pt/GH and Pt/GHA nano-

[a] *Dr. Q. Wang, M. Song, Dr. C. Chen, Prof. X. Wang*
Key Laboratory of Novel Thin Film Solar Cells
Institute of Plasma Physics, Chinese Academy of Sciences
P.O. Box 1126, 230031 Hefei (PR China)
Fax: (+86)-551-5591310
E-mail: xkwang@ipp.ac.cn

[b] *Prof. W. Hu*
Beijing National Laboratory for Molecular Sciences
Key Laboratory of Organic Solids
Institute of Chemistry, Chinese Academy of Sciences
100190 Beijing (PR China)

Supporting information for this article is available on the WWW under http://dx.doi.org/10.1002/cplu.201200070.

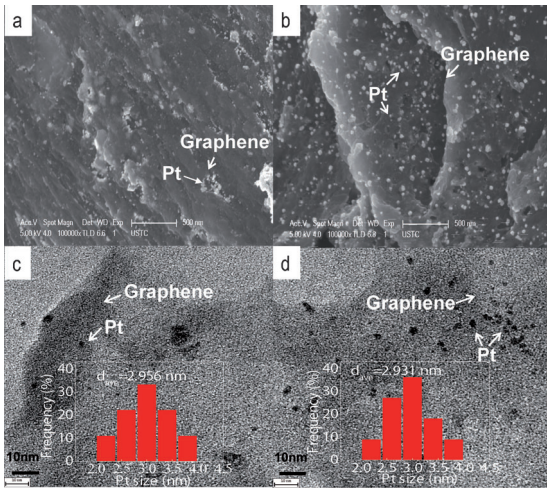

Figure 2. SEM images of (a) Pt/GH and (b) Pt/GHA. TEM images of (c) Pt/GH and (d) Pt/GHA.

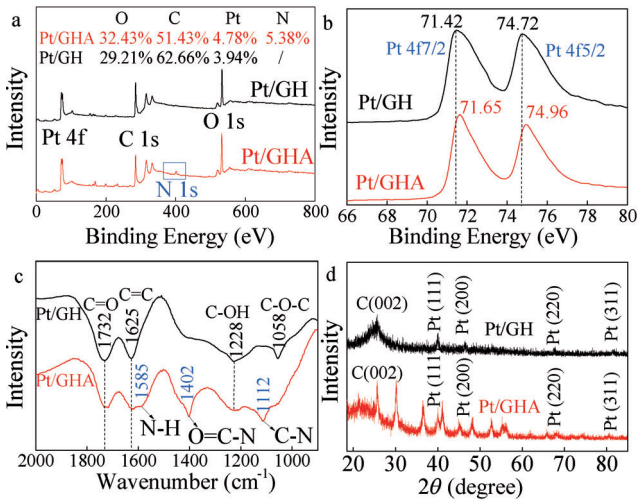

Figure 3. (a) XPS spectra of Pt/GH and Pt/GHA, (b) Pt 4f XPS spectra of Pt/GH and Pt/GHA, (c) FTIR spectra of Pt/GH and Pt/GHA, and (d) XRD patterns of Pt/GH and Pt/GHA.

structures are shown in Figure 2. The SEM images confirm that Pt NPs are successfully deposited on graphene surface. As shown in Figure 2b, Pt NPs are highly dispersed on Pt/GHA with less agglomeration. In contrast, Pt NPs on Pt/GH show a higher degree of aggregation (Figure 2a) with particle size ranging from approximately 3 nm to several tens of nanometers in diameter. The TEM image further confirms the SEM analysis, showing that a non-uniform distribution of Pt NPs on the Pt/GH surface (Figure 2c), whereas Pt NPs on Pt/GHA are homogeneous and well-dispersed (Figure 2d). Their size distribution was evaluated statistically and is shown in the inset of Figure 2c,d. The particle size of Pt distributes mainly between 2.0 and 4.0 nm with an average diameter of about 2.931 nm for Pt/GHA and 2.956 nm for Pt/GH. The AFM images show the ability to attain non-uniform high distribution of Pt NPs anchored on GH surface (Figure S1a in the Supporting Information), meanwhile the height of Pt NPs is uniform on the GHA surface (Figure S1b). These findings are in good agreement with SEM and TEM analysis. The above analyses indicate that nitrogen functional groups on GHA improve the homogeneous growth and distribution of Pt NPs on the graphene surface.

The X-ray photoelectron spectroscopy (XPS) spectra confirm the doping of Pt NPs on the graphene surface (Figure 3a). In Pt/GHA, the peaks at 71.65 eV and 74.96 eV correspond to Pt 4f, while those of Pt 4f occur at 71.42 eV and 74.72 eV in Pt/GH. The O 1s peak, which might be advantageous for catalyst of ORR electrode, is observed at 532.8 eV both in Pt/GHA and Pt/GH. It has been reported that graphene with high oxygen-group content has strong ability for O_2 adsorption, which is of additional advantage as the ORR electrode.[17] The higher ratio of O to C (0.63) in Pt/GHA than that of O to C (0.47) in Pt/GH suggests a better potential application of Pt/GHA in DMFC, which is illustrated by the electrochemistry experiment to follow. In Pt/GHA, the peak at 401.7 eV corresponds to N 1s, and the N percentage in the sample is about 5.38%. The C 1s high resolution XPS spectrum (Figure S2a) of Pt/GH shows that the peaks at 284.76 and 285.64 eV correspond to the graphite-like sp^2 carbon atoms, and the same peaks are also observed in Pt/GHA (Figure S2b). Compared with Pt/GH, the small peak at 287.1 eV in Pt/GHA is not attributed to sp^2-carbon atoms, but corresponds to sp^3-nitrogen atoms, which originated from the substitution doping of N atoms.[18] The peak at 289.0 eV is attributed to the C=O bond, thus indicating the partial removal of oxygen-containing functional groups.[19] The N 1s XPS spectrum of Pt/GHA (Figure S3a) can be further deconvoluted into three peaks at 397.93, 400.30, and 401.92 eV, which correspond to pyridinic N, pyrrolic N, and graphitic N atoms, respectively. This finding suggest that the N atoms are in three different bonding characteristics when that are inserted into the graphene network (Figure S3b),[6,17] and all of them play important roles in the electrocatalytic process.[5a,20] In the Pt 4f XPS spectrum of Pt/GHA, the strong ligand effect[21] between Pt NPs and GHA is evidenced by the shift of the Pt $4f_{7/2}$ peak (71.65 eV) to a higher binding energy as compared with the Pt $4f_{7/2}$ peak (71.42 eV) in Pt/GH. In addition, the peak of Pt $4f_{5/2}$ at 74.96 eV in Pt/GHA is also higher than that of Pt $4f_{5/2}$ at 74.72 eV in Pt/GH (Figure 3b). Although the nature of Pt deposition is not well understood, it is plausible to hypothesize that the interaction between Pt and GHA is enhanced, and thus causes the shift of the Pt 4f peak to higher binding energies, thereby creating a stabilizing effect against Pt oxidation/dissolution.[22]

The residual oxygen and nitrogen functional groups on the surfaces of Pt/GH and Pt/GHA are confirmed by the FTIR spectra (Figure 3c). The characteristic features of Pt/GH are the absorption bands corresponding to the C–O stretching at 1058 cm^{-1}, the C–OH stretching at 1228 cm^{-1}, and the C=O carbonyl stretching vibrations at 1732 cm^{-1}. The band at 1625 cm^{-1} corresponds to the C=C sp^2 character.[23] In the FTIR spectrum of Pt/GHA, new bands appear strongly at 1402 cm^{-1} and 1112 cm^{-1}, which correspond to the introduced C–N by the NH_3 plasma treatment, and the band at 1585 cm^{-1} is assigned to the N–H stretch of the amine group. Residual

oxygen functional groups at 1732 cm^{-1}, 1625 cm^{-1}, and 1228 cm^{-1} are also detected. It is necessary to note that the band at 1625 cm^{-1} is attributed to aromatic C=C bonds in the two samples, and thus indicates that the plasma treatment is so mild that the graphene network is maintained. The FTIR analysis is in good agreement with the C 1s XPS analysis. The XRD patterns of Pt/GH and Pt/GHA (Figure 3 d) exhibit the characteristic face-centered cubic (fcc) platinum lattice: diffraction peaks at 39.6° for Pt(111), 46.2° for Pt(200), 67.3° for Pt(220), and 81.4° for Pt(311). These peaks confirm that the H_2PtCl_6 precursors have been reduced to Pt NPs and then are successfully deposited on graphene by plasma treatment.[24] Furthermore, the XRD patterns exhibit either negligible peak in Pt/GHA or a low-intensity peak in Pt/GH at $2\theta = 25°$. As is well known, carbon black and graphite have a broad diffraction peak for C(002) at $2\theta = 25°$ and is interpreted in terms of short-range order in stacked graphene sheets.[25] In Pt/GHA, the diffraction peak for C(002) is negligible, thus indicating that significant face-to-face stacking is absent.[8a] In Pt/GH, the low intensity for C(002) also indicates that the carbon atoms are amorphous or have low levels of graphitization.[26]

As discussed above, the surface treatment of graphene by plasma has a major role on the growth of Pt NPs. The nucleation of Pt NPs with homogeneous distribution at GHA surfaces should be mainly governed by the presence of nitrogen and oxygen groups, which greatly improve the Pt NPs attachment to graphene surfaces. Graphene oxide has a large amount of oxygen groups on its surface, the plasma treatment results in a decomposition of the hydroxyl and epoxide groups of GO.[27] Although in this case, because the plasma treatment is carried out under mild condition it is not enough for the complete reduction of the oxygen groups (C=O band at 1732 cm^{-1} in IR spectrum and C 1s XPS spectrum), and it maintains the graphene network as much as possible (C=C band at 1625 cm^{-1} in IR spectrum and C 1s XPS spectrum). Furthermore, ammonia plasma can introduce new functional groups (C–N bands at 1402 cm^{-1} and 1112 cm^{-1} in the FTIR spectrum and N 1s in the XPS spectrum) on graphene surfaces.

The electrocatalytic activities of Pt/GH and Pt/GHA were examined. Figure 4 a shows the cyclic voltammogram (CV) curves of the electrodes purged in 1 M H_2SO_4. The electrochemical active surface areas (ECSA) of Pt/GH and Pt/GHA can be obtained by using hydrogen adsorption/desorption methods with Equation (1):[28]

$$S_{ECSA} = \frac{Q_H}{0.21 \times L} \quad (1)$$

where S_{ECSA} represents the ECSA value ($cm^2\,mg^{-1}$), Q_H ($mC\,cm^{-2}$) is the charge transfer during the electrodesorption of H_2 on Pt sites, and L ($mg\,cm^{-2}$) is the amount of Pt NPs loading on the electrode, and 0.21 ($mC\,cm^{-2}$) is the charge required to oxidize a monolayer of H_2 on smooth surface of Pt NPs. The Pt/GHA shows a larger active surface area than Pt/GH. It is found that the ECSA of Pt/GHA (129.98 $m^2\,g^{-1}$) is much higher than that of Pt/GH (76.77 $m^2\,g^{-1}$), and those of Pt-based materials such as Pt/graphene (44.6 $m^2\,g^{-1}$),[8d] Pt/graphene oxide

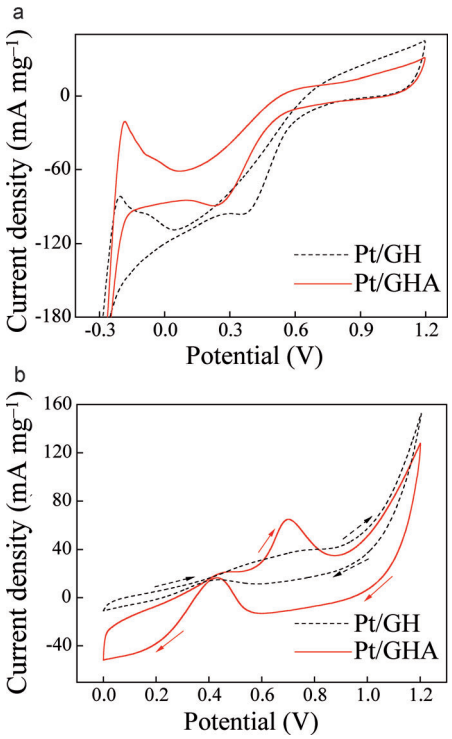

Figure 4. CV curves of Pt/GH and Pt/GHA with a scanning rate of 50 $mV\,s^{-1}$ in (a) 1 M $H_2SO_{4(aq)}$ and (b) 1 M $CH_3OH_{(aq)}$ + 0.5 M $H_2SO_{4(aq)}$.

(16.9 $m^2\,g^{-1}$), carbon black supported Pt (19 $m^2\,g^{-1}$),[29] Pd–Pt bimetallic nanodendrites (57.1 m^2g^{-1}),[30] Pd–Pt/graphene (81.6 $m^2\,g^{-1}$), commercial Pt/C (74.0 $m^2\,g^{-1}$),[31] Pt/[carbon nanotubes (CNTs)-ionic liquid polymer] (71.4 $m^2\,g^{-1}$), Pt/CNTs (47.1 $m^2\,g^{-1}$), Pt–Ru/CNTs (53.5 $m^2\,g^{-1}$),[32] Pt dispersed on functionalized graphene and functionalized multiwall carbon nanotube [Pt/(f-G-f-MWNT)] hybrid (108 $m^2\,g^{-1}$),[33] mesoporous Pt with giant mesocages (74 $m^2\,g^{-1}$),[34] Pt/chemically converted graphene (36.3 $m^2\,g^{-1}$), Pt/MWCNT (33.4 $m^2\,g^{-1}$),[35] Pt nanowires/Sn@CNT (17.2 $m^2\,g^{-1}$),[36] and Pt/reduced GO (55.5 $m^2\,g^{-1}$).[37]

The electrooxidation of methanol is characterized by CV measurements as shown in Figure 4 b. The nitrogen atoms introduced to GHA can enhance the electronic property of graphene nanosheets as expected. When the scan is from 0 to 1.2 V, the forward oxidation current peak (I_f) of methanol on Pt/GHA appears at 0.70 V, which is shifted to negative direction by approximately 80 mV in comparison with Pt/GH (0.78 V). In the reverse potential scan, the scan is from 1.2 to 0 V, a reverse anodic current peak appears at about 0.43 V for the two catalysts. The reverse anodic peak (I_b) is attributed to the oxidation of incompletely oxidized carbonaceous species formed in the forward scan.[38] The I_f value of methanol oxidation on Pt/GH electrode reaches 40.22 $mA\,mg^{-1}$, which is only approximately 62% of that on the Pt/GHA electrode (64.98 $mA\,mg^{-1}$). The higher anodic current of Pt/GHA can be attributed to the surface functionalities especially to the nitrogen groups, thus indicating an enhanced methanol oxidation activity than that of Pt/GH. The ratio of the I_f to I_b is a key index of the catalyst tolerance toward the poisoning species such as adsorbed CO in-

termediates formed by the decomposition of methanol.[31,37–41] A higher ratio implies more effective removal of the poisoning species on the catalyst surface. In our study, the I_f/I_b ratio of Pt/GHA is 3.95, which is higher than that of Pt/GH (2.72), and much higher than those of Pt/graphene-PDDA catalyst (1.92),[16a] the three-dimensional Pd–Pt bimetallic nanodendrites supported on graphene (1.25),[31] Pt/chemically converted graphene (0.83),[35] Pt/reduced GO (2.6),[37] the commercial E-TEK catalyst (0.74), Pt–CNT catalyst (0.88),[39] and Pt/CNT synthesized in supercritical fluid catalysts (1.4).[40] The result indicates that the Pt/GHA has less carbonaceous accumulation, much more improved CO tolerance, and effective removal of the poisoning intermediates in the forward scan.[40] Moreover, the onset potential for methanol oxidation on Pt/GHA and Pt/GH start at 0.01 V, which is shifted more negative than other reported catalysts such as Pt/graphene-PDDA (0.10 V),[16a] Pt/graphene (0.2 V),[8d] Pt/chemically converted graphene (0.38 V),[35] Pt/reduced GO (0.5 V),[37] and 3D dendritic platinum (0.44 V),[41] thus demonstrating the excellent electrocatalytic activity of Pt/GHA nanocomposites toward methanol oxidation.

Based on the results outlined above, several explanations are proposed for the high catalytic activity of Pt/GHA nanocomposites: 1) it most likely a result of the uniform and small particle size of Pt NPs and their well dispersion on the GHA supports. The nitrogen groups introduced on the graphene surface by NH_3 plasma facilitate the Pt NPs dispersion and prevent their agglomeration. Moreover, those oxygen and nitrogen groups on the large specific surface of graphene help the so-called cooperative self-assembly of Pt NPs with the support;[42] 2) the excellent electron conductivity provided by graphene supports might accelerate the reaction kinetics and accelerate the methanol and O_2 diffusion;[36] 3) previous studies of Pt-based nanoparticle catalysts reveal that an oxygen-containing surface can remove the strongly absorbed poisonous species (such as CO, $HCOO^-$, and HCO^-);[36,43] 4) as the graphene surfaces are bombarded with high-energy ion beams, carbon vacancy defects and interstitial defects are produced,[44] which can absorb several kinds of molecules (such as O_2, CO, H_2O) and effectively dissociate H_2O to H and OH species.[45,46] This significantly accelerates the ability of the Pt/GHA for CO oxidation. Therefore, the improved catalytic activity and CO tolerance are observed that may originate partially from the unique plasma-treated GHA supports. For these reasons, it is expected that the grown of Pt NPs on plasma-treated graphene supports can combine many advantageous factors such as good dispersion of Pt NPs and excellent properties for catalyst supports.

In summary, we have developed a facile plasma approach for the synthesis of Pt/GH and Pt/GHA catalysts under mild conditions. The functional graphenes (GH and GHA) are also prepared by the simple and environmental friendly plasma treatment which can avoid using needless chemical reagent though the processes. Compared with Pt/GH and other reported Pt-based electrodes, the Pt/GHA electrodes show a higher electrochemically active surface area, better tolerance toward CO, the negative shift of forward peak potential and onset potential, accompanied by obvious enhanced I_f and the ratio of I_f/I_b, and thus, exhibit excellent electrocatalytic activity toward methanol electrooxidation. The simultaneous in situ reduction and effective functionalization under mild conditions makes this approach promising and exciting for further improving the catalyst performance of direct methanol fuel cells, polymer electrolyte membrane fuel cells, and supercapacitor.

Experimental Section

Preparation of GH, GHA, Pt/GH, and Pt/GHA

Graphene oxide (GO) was treated in a home-made plasma generator (Scheme S1) induced by a radio-frequency-driven inductively coupled plasma. The pressure in the reactor was evacuated to 5 Pa, and then the H_2 plasma occurring at 15 Pa was operated for 30 min to reduce the GO and afforded H-doped graphene (GH). The NH_3 plasma treated the GO for 30 min afforded N-doped graphene (GHA). The H_2 or NH_3 plasma treated of GO (i.e. GH or GHA) were then mixed with an aqueous solution of H_2PtCl_6 (1 mM) and balanced for 12 h. Then the mixture was dried at 352 K under N_2 and subsequently treated by hydrogen plasma (15 Pa) for 40 min under continuous stirring to grow Pt nanoparticles on GH or GHA surfaces, and thereby to synthesize the Pt/GH and Pt/GHA catalysts.

Characterization

Scanning electron microscopy (SEM) and transmission electron microscopy (TEM) images were obtained using JSM-6700Fand JEM-2011F, respectively. Atomic force microscopy (AFM) images were obtained using a Digital Instruments MultiMode V scanning probe microscope. The Fourier transform infrared (FTIR) spectra were recorded in pressed KBr pellets (Aldrich, 99%, FTIR grade) by using a Nicolet 8700 FT-IR spectrometer at RT. The powder X-ray diffraction (XRD) patterns of the samples were recorded on a D/Max-IIIA X-ray diffractometer (Rigaku Co., Japan) using $Cu_{K\alpha}$ ($\lambda = 1.5418$ Å). The X-ray photoelectron spectroscopy (XPS) analysis of the samples was conducted on a VG ESCALAB MKII spectrometer using an $Mg_{K\alpha}$ as the X-ray source (1253.6 eV, 120 W) at a constant analyzer-pass energy. The energy scale was internally calibrated by referencing the binding energy of the C 1s peak at 284.6 eV for contaminated carbon.

Electrochemical measurements

H_2SO_4 (1.0 M) was selected as the electrolyte for electrochemical active surface area (ECSA) analysis. Aqueous solutions of H_2SO_4 (0.5 M) and CH_4O (1.0 M) were selected for the analysis of electrooxidation of methanol. The solutions were first deaerated with N_2 before the electrochemical measurements. All electrochemical measurements were carried out using an autolab potentiostat/galvanostat (PGSTAT302N, Switzerland) at a scanning rate of 50 mV s^{-1}. A three-electrode system consisting of the catalysts as the working electrode, platinum as the counter, and a KCl saturated Ag/AgCl electrode as the reference electrode was used in all cases. A predefined amount of Pt/GH or Pt/GHA catalysts were added to 2-propanol (1 mL), which were then shaken for 30 min in an ultrasonic bath to form a slurry. Then the slurry was brushed onto a piece of carbon paper (0.4×0.6 cm; HCP020P) and dried in an oven at 80 °C for 20 min. These were later used as working electrodes. A solution of nafion (DE520; 100 μL, 5 wt%), which acted

as a protective layer to prevent catalysts loss in the solution, was spread on top of the catalysts layer and dried at 80 °C. The electrodes were activated by cycling the potential between −0.4 and 1.2 V (vs. Ag/AgCl) for ECSA measurements and between 0 and 1.2 V (vs. Ag/AgCl) for methanol electrooxidation measurements.

Acknowledgements

We gratefully acknowledge the 973 project of MOST (2011CB933700) and the National Natural Science Foundation of China (21077107, 21071147, 20971126, 91126020, 21107115, 51033006).

Keywords: electrocatalysts · graphene · nanoparticles · plasma · platinum

[1] H. L. Wang, Y. Y. Liang, Y. G. Li, H. J. Dai, *Angew. Chem.* **2011**, *123*, 11161 – 11164; *Angew. Chem. Int. Ed.* **2011**, *50*, 10969 – 10972.
[2] R. Bashyam, P. Zelenay, *Nature* **2006**, *443*, 63 – 66.
[3] J. P. Collman, N. K. Devaraj, R. A. Decreau, Y. Yang, Y. L. Yan, W. Ebina, T. A. Eberspacher, C. E. D. Chidsey, *Science* **2007**, *315*, 1565 – 1568.
[4] J. Zhang, K. Sasaki, E. Sutter, R. R. Adzic, *Science* **2007**, *315*, 220 – 222.
[5] K. P. Gong, F. Du, Z. H. Xia, M. Durstock, L. M. Dai, *Science* **2009**, *323*, 760 – 764.
[6] R. L. Liu, D. Q. Wu, X. L. Feng, K. Müllen, *Angew. Chem.* **2010**, *122*, 2619 – 2623; *Angew. Chem. Int. Ed.* **2010**, *49*, 2565 – 2569.
[7] S. Yang, X. Feng, X. Wang, K. Müllen, *Angew. Chem.* **2011**, *123*, 5451 – 5455; *Angew. Chem. Int. Ed.* **2011**, *50*, 5339 – 5343.
[8] a) Y. C. Si, E. T. Samulski, *Chem. Mater.* **2008**, *20*, 6792 – 6797; b) E. Yoo, T. Okata, T. Akita, M. Kohyama, J. Nakamura, I. Honma, *Nano Lett.* **2009**, *9*, 2255 – 2259; c) S. Stankovich, D. A. Dikin, R. D. Piner, K. A. Kohlhaas, A. Kleinhammes, Y. Jia, Y. Wu, S. T. Nguyen, R. S. Ruoff, *Carbon* **2007**, *45*, 1558 – 1565; d) Y. M. Li, L. H. Tang, J. H. Li, *Electrochem. Commun.* **2009**, *11*, 846 – 849; e) X. Z. Tang, Z. Cao, H. B. Zhang, J. Liu, Z. Z. Yu, *Chem. Commun.* **2011**, *47*, 3084 – 3086.
[9] Z. C. Liu, C. F. Yu, I. A. Rusakova, D. X. Huang, P. Strasser, *Top. Catal.* **2008**, *49*, 241 – 250.
[10] Y. J. Gan, L. T. Sun, F. Banhart, *Small* **2008**, *4*, 587 – 591.
[11] H. K. Kammler, L. Madler, S. E. Pratsinis, *Chem. Eng. Technol.* **2001**, *24*, 583 – 596.
[12] S. Eliezer, N. Eliaz, E. Grossman, D. Fisher, I. Gouzman, Z. Henis, S. Pecker, Y. Horovitz, M. Fraenkel, S. Maman, Y. Lereah, *Phys. Rev. B* **2004**, *69*, 144119.
[13] K. J. Jeon, Z. H. Lee, *Chem. Commun.* **2011**, *47*, 3610 – 3612.
[14] D. Wang, Y. Li, *Adv. Mater.* **2011**, *23*, 1044 – 1060.
[15] a) Y. G. Zhou, J. J. Chen, F. B. Wang, Z. H. Sheng, X. H. Xia, *Chem. Commun.* **2010**, *46*, 5951 – 5953; b) H. C. Gao, F. Xiao, C. B. Ching, H. W. Duan, *ACS Appl. Mater. Interfaces* **2011**, *3*, 3049 – 3057; c) S. J. Guo, Y. M. Zhai, S. J. Dong, E. K. Wang, *ACS Nano* **2010**, *4*, 3959 – 3968.
[16] a) J. D. Qiu, G. C. Wang, R. P. Liang, X. H. Xia, H. W. Yu, *J. Phys. Chem. C* **2011**, *115*, 15639 – 15645; b) M. S. Wietecha, J. Zhu, G. H. Gao, N. Wang, H. Feng, M. L. Gorring, M. L. Kasner, S. F. Hou, *J. Power Sources* **2012**, *198*, 30 – 35.
[17] L. T. Qu, Y. Liu, J. B. Baek, L. M. Dai, *ACS Nano* **2010**, *4*, 1321 – 1326.
[18] D. C. Wei, Y. Q. Liu, Y. Wang, H. L. Zhang, L. P. Huang, G. Yu, *Nano Lett.* **2009**, *9*, 1752 – 1758.
[19] D. Marton, K. J. Boyd, A. H. Al-Bayati, S. S. Todorov, J. W. Rabalais, *Phys. Rev. Lett.* **1994**, *73*, 118 – 121.
[20] R. T. Lv, T. X. Cui, M. S. Jun, Q. Zhang, A. Y. Cao, D. S. Su, Z. J. Zhang, S. H. Yoon, J. Miyawaki, I. Mochida, F. Y. Kang, *Adv. Funct. Mater.* **2011**, *21*, 999 – 1006.
[21] Y. Liang, H. Zhang, H. Zhong, X. Zhu, Z. Tian, D. Xu, B. Yi, *J. Catal.* **2006**, *238*, 468 – 476.
[22] S. G. Chen, Z. D. Wei, L. Guo, W. Ding, L. C. Dong, P. K. Shen, X. Q. Qi, L. Li, *Chem. Commun.* **2011**, *47*, 10984 – 10986.
[23] a) A. B. Bourlinos, D. Gournis, D. Petridis, T. Szabó, A. Szeri, I. Dékány, *Langmuir* **2003**, *19*, 6050 – 6055; b) J. I. Paredes, S. Villar-Rodil, A. Martínez-Alonso, J. M. D. Tascón, *Langmuir* **2008**, *24*, 10560 – 10564.
[24] M. Carmo, V. A. Paganin, J. M. Rosolen, E. R. Gonzalez, *J. Power Sources* **2005**, *142*, 169 – 176.
[25] F. Su, J. Zeng, X. Bao, Y. Yu, J. Lee, X. S. Zhao, *Chem. Mater.* **2005**, *17*, 3960 – 3967.
[26] Z. X. Yang, Y. D. Xia, R. Mokaya, *J. Am. Chem. Soc.* **2007**, *129*, 1673 – 1679.
[27] M. J. McAllister, J. L. Li, D. H. Adamson, H. C. Schniepp, A. A. Abdala, J. Liu, M. Herrera-Alonso, D. L. Milius, R. Car, R. K. Prud'homme, I. A. Aksay, *Chem. Mater.* **2007**, *19*, 4396 – 4404.
[28] A. Pozio, M. D. Francesco, A. Cemmi, F. Cardellini, L. Giorgi, *J. Power Sources* **2002**, *105*, 13 – 19.
[29] B. Seger, P. V. Kamat, *J. Phys. Chem. C* **2009**, *113*, 7990 – 7995.
[30] B. Lim, M. J. Jiang, P. H. C. Camargo, E. C. Cho, J. Tao, X. M. Lu, Y. M. Zhu, Y. N. Xia, *Science* **2009**, *324*, 1302 – 1305.
[31] S. J. Guo, S. J. Dong, E. K. Wang, *ACS Nano* **2010**, *4*, 547 – 555.
[32] B. H. Wu, D. Hu, Y. J. Kuang, B. Liu, X. H. Zhang, J. H. Chen, *Angew. Chem.* **2009**, *121*, 4845 – 4848; *Angew. Chem. Int. Ed.* **2009**, *48*, 4751 – 4754.
[33] R. I. Jafri, T. Arockiados, N. Rajalakshmi, S. Ramaprabhu, *J. Electrochem. Soc.* **2010**, *157*, B874 – B879.
[34] Y. Yamauchi, A. Sugiyama, R. Morimoto, A. Takai, K. Kuroda, *Angew. Chem.* **2008**, *120*, 5451 – 5453; *Angew. Chem. Int. Ed.* **2008**, *47*, 5371 – 5373.
[35] Y. J. Li, W. Gao, L. J. Ci, C. M. Wang, P. M. Ajayan, *Carbon* **2010**, *48*, 1124 – 1130.
[36] S. H. Sun, G. X. Zhang, D. S. Geng, Y. G. Chen, M. N. Banis, R. Y. Li, M. Cai, X. L. Sun, *Chem. Eur. J.* **2010**, *16*, 829 – 835.
[37] S. Sharma, A. Ganguly, P. Papakonstantinou, X. P. Miao, M. X. Li, J. L. Hutchison, M. Delichatsios, S. Ukleja, *J. Phys. Chem. C* **2010**, *114*, 19459 – 19466.
[38] Y. Z. Chang, G. Y. Han, M. Y. Li, F. Gao, *Carbon* **2011**, *49*, 5158 – 5165.
[39] Y. Y. Mu, H. P. Liang, J. S. Hu, L. Jiang, L. J. Wan, *J. Phys. Chem. B* **2005**, *109*, 22212 – 22216.
[40] Y. H. Lin, X. L. Cui, C. Yen, C. M. Wai, *J. Phys. Chem. B* **2005**, *109*, 14410 – 14415.
[41] L. Wang, Y. Yamauchi, *Chem. Mater.* **2009**, *21*, 3562 – 3569.
[42] Y. H. Jang, S. Y. Yang, Y. J. Jang, C. Park, J. K. Kim, D. H. Kim, *Chem. Eur. J.* **2011**, *17*, 2068 – 2076.
[43] R. Mancharan, J. B. Goodenough, *J. Mater. Chem.* **1992**, *2*, 875 – 887.
[44] J. R. Hahn, H. Kang, *Phys. Rev. B* **1999**, *60*, 6007 – 6017.
[45] P. Cabrera-Sanfelix, G. R. Darling, *J. Phys. Chem. C* **2007**, *111*, 18258 – 18263.
[46] A. Allouche, Y. Ferro, *Carbon* **2006**, *44*, 3320 – 3327.

Received: March 25, 2012
Published online on April 11, 2012

